Journal of Molecular Structure 1261 (2022) 132902

Contents lists available at ScienceDirect

Journal of Molecular Structure

journal homepage: www.elsevier.com/locate/molstr

New silver(I) complex as antibiotic candidate: Synthesis, spectral characterization, DFT, QTAIM and antibacterial investigations and docking properties

Sibel Celik[a,*], Senay Yurdakul[b], Belgin Erdem[a]

[a] Vocational School of Health Services, Kırsehir Ahi Evran University, Kırşehir 40100, Turkey
[b] Department of Physics, Faculty of Science, Gazi University, Ankara, Turkey

ARTICLE INFO

Article history:
Received 29 January 2022
Revised 20 March 2022
Accepted 21 March 2022
Available online 22 March 2022

Keywords:
4-pyridinecarboxaldehyde
Antibacterial
Antiquorum-sensing
Molecular docking
AIM
DFT

ABSTRACT

In the present work, a newly synthesized silver(I) complex was characterized using elemental analysis, UV–Vis spectroscopy, and infrared spectroscopy. DFT calculations at the B3LYP/LANL2DZ level were used to investigate structural, electronic, and spectroscopic properties. The intermolecular interactions in the structure were analyzed by topological AIM, RDG, and NBO approaches. Compound [Ag(4-pyridinecarboxaldehyde)$_4$]NO_3 proved to be the most active compound in this study and showed the highest antibacterial activity against *S. aureus* ATCC 29,213, *S. epidermidis* ATCC 35,984 and *P. aeruginosa* ATCC 27,853. Test compound was examined for antiquorum-sensing activity against *C. violaceum* ATCC 12,472 and title compound exhibited good antiquorum-sensing activity. In addition, these compound activity relationships were further supported by *in-silico* molecular docking studies where some of the active title compound showed maximum dock score.

1. Introductions

The discovery of new heterocyclic ligands for the purpose of synthesizing novel metal complexes has sparked considerable interest due to the many uses of coordination chemistry in a variety of fields, such as medicine, hydrometallurgy, and biotechnology [1]. The 4-pyridinecarboxaldehyde ligand and its metal complexes are considered privileged ligands in medicinal chemistry because they have been shown to have a wide range of biological properties [2]. It has been discovered to have good action against bacteria (e.g., *Staphylococcus aureus, Escherichia coli, Klebsiella pneumoniae*) and fungus (*Candida albicans, Apergillus niger,* and *Pencillium sp.*) [3–5], as well as modest nuclease activity [5]. Silver is utilized in clinical practice because it is efficient against a wide spectrum of bacteria at low doses [6–8]. Also, silver has the capacity to bind thiols in proteins and enzymes, inhibit cellular respiration, damage cell membranes, and bind nucleic acids [9]. There is a great deal of interest in developing new silver(I) compounds with high pharmacological activity, such as antitumor [10,11] and anticancer agents [12,13], anti-ulcer, antibacterial, and antifungal [12–14] properties, based on the benefits of silver(I) and emerging challenges in illness therapy. This is part of a larger effort to develop new medications to complement existing ones and increase the battle against illnesses.

In the literature, the synthesis and theoretical analysis of 4-pyridinecarboxaldehyde (4-PCA) and its complexes with Co (II), Ni (II), Cu (II), and Zn (II) ions have been reported [1,15,16]. The biological importance of the Schiff base complexes, as well as their medicinal applications, has made them a fascinating and rewarding study target, inspiring scientists for further studies.

In this study, the 4-pyridinecarboxaldehyde silver nitrate complex, [Ag(4-PCA)$_4$]NO_3, was synthesized. To characterize the title compound, quantum chemical calculations and wave function analysis techniques were applied. The title compound's optimized geometrical structure was determined using the Gaussian 09 W software. Vibrational wavenumbers were calculated for the complex by using experimental (FT-IR and UV-vis) and theoretical methods. The molecular electrostatic potential (MEP) surface was analysed. The chemical reactivity Fukui function and NBO analysis were also carried out to understand the reactive sites of the Ag(I) complex. The topological analysis was carried out using color-filled and relief maps of Atoms in Molecule (AIM), reduced density gradient (RDG), electron localization function (ELF), and localized orbital locator (LOL). Molecular docking of the title ligand is performed with anti-bacterial receptor proteins. Also, computer-aided drug design can predict pharmacokinetics and pharmacology features such as absorption, metabolism, excretion (ADME), and toxicity of the title silver complex.

* Corresponding author.
E-mail address: sibelcelik@ahievran.edu.tr (S. Celik).

https://doi.org/10.1016/j.molstruc.2022.132902
0022-2860/

2. Experimental

2.1. Synthesis of complex

Silver nitrate and 4-pyridinecarboxaldehyde were purchased from Sigma-Aldrich and used without purification. The chemical process was used to create a silver complex. The ligand (4-PCA) (2 mmol), was liquefied in 20 mL of ethanol. Following that, $AgNO_3$ (1 mmol) was gradually added to the first obtained solution with constant mixing at 50 °C. After 3 h of stirring at the same temperature, the final solution was kept at room temperature for 1 week to allow the solvent to evaporate. To protect the combination from light, it was covered in aluminum foil and stored at +4 °C for three months. The synthesized compound contains a 1:4 metal-to-ligand ratio. The colorless metal complex was filtered and dried under an ambient atmosphere. The yield of the synthesized compound was 75.4%. The following calculated and experimental values for C, H, and N analyses were reported:$[Ag(C6H5NO)_4]NO_3$, [C24H20AgN5O7], CHN Calc: C: 48.17%, H: 3.36%, N: 11.70%. Found: C: 48.80%, H: 4.01%, N: 11.40%.

2.2. Instrumentation for recording spectra

The infrared spectrum of $[Ag(4\text{-}PCA)_4]NO_3$ complex was recorded between 4000 and 550 cm^{-1} on the Bruker Vertex 80 FT-IR spectrometer. Far-IR spectra was recorded between 700 and 100 cm^{-1} on the Bruker IFS 66/S system. UV–Vis spectra were recorded in quartz cell DMSO as the solvent using an Agilent HP 8453 spectrophotometer.

2.3. Antibacterial and antiquorum-sensing activities

Ten bacterial cultures (*S. aureus* ATCC 29,213, *S. epidermidis* ATCC 35,984, *L. monocytogenes* ATCC 35,152, *B. subtilis* ATCC 6633, *B. cereus* 709 Roma, *E. faecalis* ATCC 29,212, *E. coli* ATCC 25,922, *S. typhimurium* ATCC 14,028, *P. aeruginosa* ATCC 27,853 and *K. pneumoniae* ATCC 13,883 were used. All these bacteria were taken from cultures obtained from Kırşehir Ahi Evran University, Biology Department Culture Collection.

In this study, the antibacterial activities of compounds were determined by the Minimal inhibitor concentration (MIC) and Agar well diffusion method.

Minimum inhibitory concentrations (MIC) for compounds against bacteria strains examined in accordance with the NCCLS guideline [17]**.** Mueller-Hinton broth was used in suspension of bacteria (0.5McFarland), in solutions of substances to be tested (1000 µg/ml in DMSO) and in MIC testing.

In Agar well diffusion method, Test bacteria were inoculated into Nutrient Broth (Difco) and incubated at 37 °C for 24–48 h. Mueller Hinton Agar (Oxoid) was used in agar well diffusion method and to count bacteria (10^5 bacteria per mL) for 24–48 h. The wells of the culture plates were drilled with a sterile cork borer (7 mm diameter).

10% DMSO (10 mg /mL) dissolved compounds were added to these wells. After 24–48 h, the inhibition zones formed on the agar plates were measured in millimeters (mm).

Ampicillin (AMP) (10 µg) was used as a positive control, and DMSO was used as a negative control. The NCCLS guidelines were used for each step of the disk diffusion method [18]**.**

The test was done in triplicate and the results were expressed as a mean. The zone diameters of the obtained agar well diffusion were compared with the standard antibiotic ampicillin.

In addition, the antipathogenic potential of the compounds was detected by antiquorum detection activities against *C. violaceum* ATCC 12,472 in LB agar medium.

C. violaceum (1×10^6) culture was spread on the LB agar surface by swap. Then, wells were drilled in LB agar using cork borer and the tested compounds (5 mg / mL) were applied to the wells after dissolving in 10% DMSO.

The plates were incubated at 30 °C for 24 h to determine inhibition of pigment production around the well. The formation of a clear halo around the disc and the formation of bacterial growth inhibition were evaluated as positive.

3. Computational methods

3.1. Computational details

The DFT calculations were performed using GAUSSIAN 09 [19]. The DFT-B3LYP approach with the LANL2DZ basis set was used to optimize the geometry of the $[Ag(4\text{-}pyridinecarboxaldehyde)_4](NO_3)$ complex. The B3LYP/LANL2DZ optimized molecular structure is used to perform vibrational frequencies, HOMO-LUMO orbitals, global chemical reactivity parameters, Fukui functions, NBO, and MEP analysis of the studied compound. HOMO, LUMO, and MEP analysis were visualized using GaussView 5.0 [20]. By employing Multiwfn [21] and the molecular visualization program VMD [22], RDG analysis leads to an easy-to-catch pictorial visualization of different kinds of non-covalent interactions directly in real space.

Using the Multiwfn software based on the quantum theory of AIM, the H-bond interactions were described in terms of electron density, $\rho(r)$, its Laplacian $\nabla^2\rho(r)$ and potential energy density at bond critical points (BCP) [23,24]. ELF and LOL were graphically plotted by the non-covalent interaction (NCI) methods using the Multiwfn program.

The UV–vis spectra and features such as electronic transitions, excitation energy, absorbances, and oscillator strength of the optimized structure were calculated using the time-dependent functional theory (TD-DFT) [25] via the B3LYP/LANL2DZ method in DMSO solvent.

The molecular docking of the chemical ligand-protein binding site was performed using Autodock 2.2.6 software [26]. The docked complexes were visualized using Chimera [27] and Discover studio software [28].

Pre-ADMET software [29] and the SwissADME tool [30] are used to calculate the ADME properties of the title complex. The organ toxicities and toxicological end points of the Ag(I) complex, as well as their LD_{50}, were estimated using the Protox-II website [31].

4. Results and discussion

4.1. Molecular geometry

The B3LYP/LANL2DZ method was used to calculate the optimized molecular structural parameters (bond lengths and bond angles), and the results are given in Table S1. The atom numbering scheme used for $[Ag(L)_4]NO_3$ is depicted in Fig. 1. Silver most commonly forms complexes of linear and tetrahedral geometry [32], while complexes of higher coordination numbers are rare. The silver(I) centers in the compound are tetra-coordinated via distorted tetrahedral geometry via the N_{py} atoms. This complex is coordinated with two short and two long Ag−Npy bonds. The Ag−N (pyridine) bond distances are found to be: Ag-N3 = 2.286 Å, Ag-N22 = 2.264 Å, it is observed that the Ag−N bonds have good agreement with the Ag-N bonds of similar system [33–36]. However, the long bonds were so long (2.5 Å) that the complex is actually two-coordinate. It may be recalled that trans-geometry having four short bonds are not possible for these ligands due to

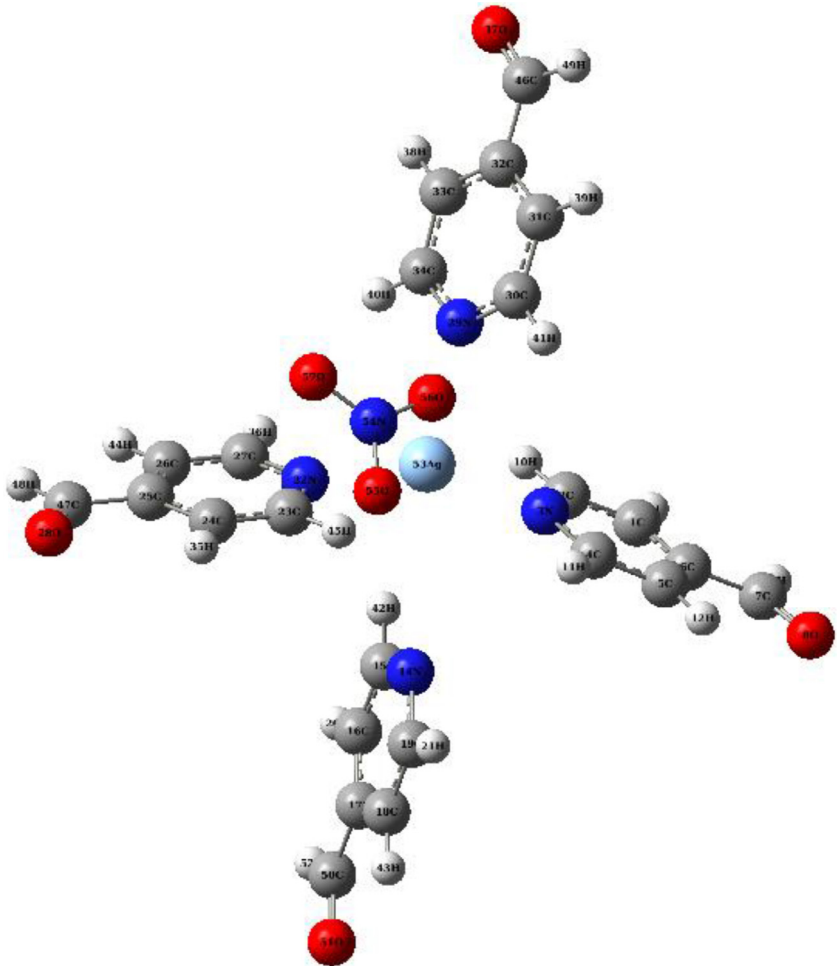

Fig. 1. Optimized geometric structure with atom numbering of the title compound.

α-hydrogen strain (bulk effect) [36]. The bond angles of N3–Ag–N22, N3–Ag–N29, and N3–Ag–N14 were 153.18°, 98.16°, and 75.51°, respectively, which were similar to previously described silver(I) complexes with N, Nbis (pyridyl) ligands [35].

The Ag...O (nitrate ion (NO_3^-)) distances are in the range of 2.56–3.85 Å indicating ionic NO3$^-$anion. The NO_3^-anion is linked to the cation complex through electrostatic interactions, intermolecular C–H···O interaction is formed between the pyridine ring carbon of 4-PCA and the nitrate ion (NO_3^-) oxygen. The intramolecular hydrogen bonding C-H…O in complex is corroborated by intermolecular hydrogen distance of H....O (2.206, 2.177, 2.241, 2.250 Å) which is shorter than the van der Waals separation between O and H atom (3 Å) [37,38]. This shows that the possibility of C–H....O hydrogen bonding and interaction exists in the Ag complex. These intramolecular interactions and the development of molecules with improved biological profiles.

4.2. Vibrational analysis

The goal of vibrational analysis on the [Ag(4-pyridinecarboxaldehyde)$_4$]NO_3 complex is to identify vibrational modes related to relevant and specific molecular structures of the compound under investigation. Fig. 2 shows both experimental and theoretical FT-IR spectra of the titled complex. Only total energy distribution (TED) contributions of ≥10% and the experimental IR and Raman spectrum were considered in the assignments. Table S2 summarizes the observed and computed wavenumbers and assignments for complex in the gas phase using the B3LYP/LANL2DZ method. The infrared spectrum confirms the existence of functional groups and can be used to gain more information about the elaborated material. Infrared (IR) analysis suggests a bidentate coordination of 4-PCA to silver by the nitrogen of the pyridine group and also confirms the presence of free nitrate anion. The most essential groups' assignments are discussed in detail.

4.2.1. C–H vibrations

In the 3100–3000 cm^{-1} region, hetero aromatics such as pyrazines, pyridines, pyrroles, furans, and thiophenes display C-H stretching bands [39]. Additionally, Cluyts et al. observed an aldehyde group C-H stretching vibration in the infrared spectra of the 4-pyridinecarboxaldehyde molecule at 2843–2704 cm^{-1} [40]. C-H stretching vibration is attributed to the band observed at 3260 and 3031 cm^{-1} (pyridine ring), and 2837 cm^{-1} (aldehyde group) in the IR spectrum in our studies. C-H stretching vibrations have been calculated to be in the range of 3126–3069 cm^{-1} and 2881–2870 cm^{-1}, respectively. The intramolecular C-H...O interaction is responsible for the deviation in experimental wavenumber from the expected range. The intermolecular hydrogen bond (C-H … O), the O-H stretching vibrations are in the range between 3500 and 3200 cm^{-1} [41,42]. The scaled values for these stretching vibrations in the complex were calculated in the 3116–3082 cm^{-1} range and are shown in Table. The CH-in plane bending and CH-out plane bending vibrations are predicted to appear in aromatic compounds in the ranges of 1400–1000 cm^{-1} and 1000–750 cm^{-1} [43,44]. The IR spectrum of the investigated Ag(I) complex shows CH in plane bending modes at 1476, 1468, 1449, and 1414 cm^{-1}, while CH-

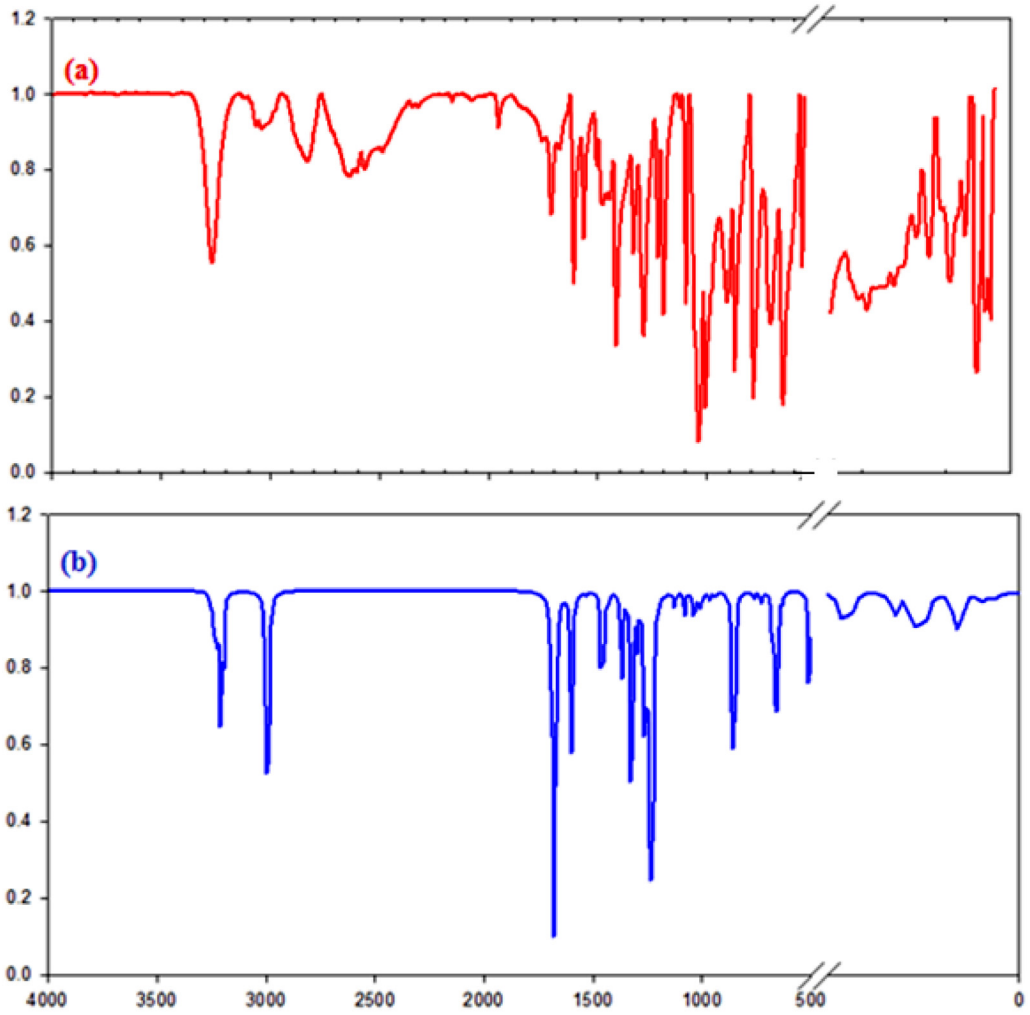

Fig. 2. FT-IR spectra of the title compound carried out experimentally (a) and theoretically (b).

out of plane bending vibrations show strong bands at 1035 and 870 cm^{-1}.

4.2.2. C=O, c-n and c-c vibrations

The C=O stretching vibrations of ketones, aldehydes, and amides generally show up in the region of 1750–1650 cm^{-1} [45]. The IR spectrum of the complex is characterized mainly by two strong bands at 1711 and 1614 cm^{-1} and calculations give this mode at 1618 and 1614 cm^{-1}, which are attributed to the carbonyl (C=O) stretching vibration. The presence of a carbonyl group is indicated by a strong band in the free ligand at 1708 cm^{-1}, while this peak was observed at 1711 cm^{-1} in the complex. The spectral analysis shows that no significant shift is observed in the carbonyl band of title complex. The fact that this band do no shift indicates that the carbonyl oxygen atoms of the ligand are non-coordinated to the metal atom in complex. Because of the possibility of X-Y...Z hydrogen bonding, there is a small deviation between experimental and theoretical wavenumbers.

The IR spectra of the ligand showed the presence of υ(C=N) stretching band at 1595 cm^{-1}. The synthesized complex, the (C=N) band appeared around 1614 cm^{-1} in the spectra. The band shifted to higher frequency after complexation, which this shifted due to the coordination of the Npy to the Ag(I) ion. In general, C-N vibrations are difficult to identify because they occur in a complicated region of the vibration spectrum that can combine many bands, for example, the carbonyl group's in-plane and out-of-plane bending vibrations. The C–N stretching bands of the aromatic ring should be in the range of 1450–950 cm^{-1} [46]. The title compound, the medium band observed at 1333 cm^{-1} and the very strong band observed at 1006 cm^{-1} in the IR spectrum are assigned to C–N stretching vibration, the relating band at 1318, 1007 cm^{-1} by DFT calculations. The IR spectrum of the free ligand demonstrates characteristic bands at 1320 and 995 cm^{-1} which we allocate to the pyridine ring C-N stretching frequencies. This band shifts to higher frequencies in the metal complex to the extent of 10–20 cm^{-1}, implying that pyridine nitrogen is involved in the coordination sphere, while the complex's elemental analysis supports this interpretation.

The C-C stretching pyridine ring vibrations arise in the region of 1600–1450 cm^{-1} in the IR spectrum [38,47]. The C-C stretching mode is recorded in the FT-IR spectrum at 1563, 1225 cm^{-1} as a medium band. The theoretical computed wavenumbers are at 1565, 1220 cm^{-1} with a TED contribution of about 25%. Normally, the C-C-C bending bands are below 600 cm^{-1}. This band, observed at 560 (medium) cm^{-1} in the IR of the title compound, is assigned to the C-C-C bending and C-C-N torsion modes.

4.4.3. NO_3 vibrations

The infrared spectra of the nitrate complexes revealed the characteristic IR frequency for the strong band at 1289 cm^{-1} in the spectrum of the metal complex confirms the presence of free $NO3^-$ as a counterion ion [48]. In the experimental IR of the Ag(I) com-

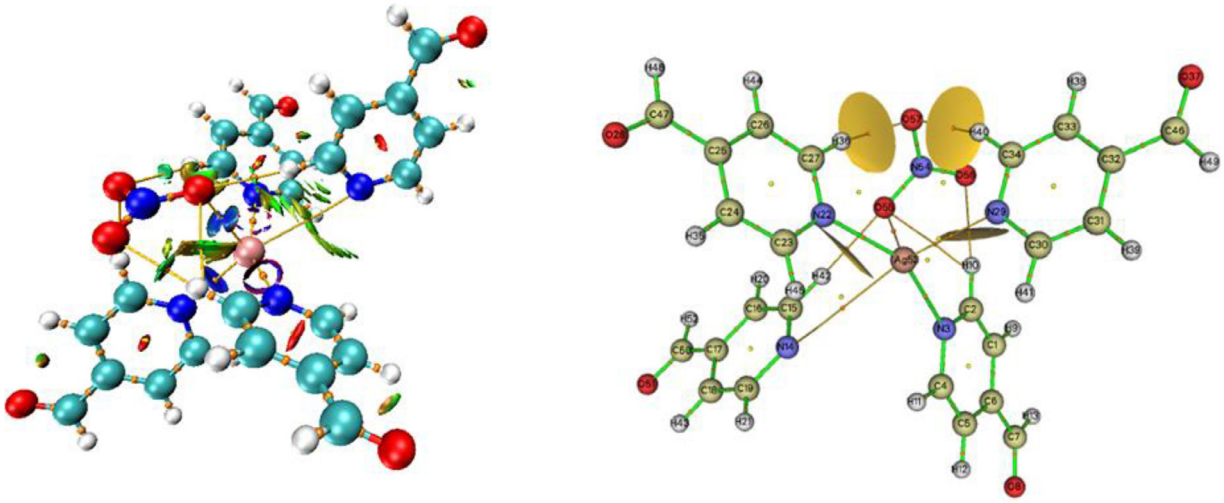

Fig. 3. Gaphical representations of the AIM analysis of the $[Ag(4\text{-}PCA)_4]NO_3$.

Table 1
AIM topological parameters for intramolecular interaction in $[Ag(4\text{-}PCA)_4]NO_3$.

Interactions	$\rho(r)$	$\nabla^2\rho(r)$	$H(r)$	$G(r)$	$V(r)$	E_{bond}(kj/mol)	λ_1	λ_2	λ_3
C_{27}-H_{36}. . .O_{57}	0.01582	0.05102	0.00166	0.01109	−0.00942	49.46442	−0.01799	−0.01709	0.08612
C_{34}-H_{40}. . .O_{57}	0.01635	0.05464	0.00176	0.01189	−0.01013	53.19263	−0.01181	−0.01746	0.09022
C_{15}-H_{42}. . .O_{55}	0.01111	0.04513	0.00207	0.009212	−0.00714	37.49214	−0.01102	−0.09780	0.06513
C_2-H_{10}. . .O_{56}	0.01442	0.04639	0.00153	0.01006	−0.00853	44.79103	−0.01157	−0.01511	0.07725

plex, a very strong band appears at 1289 cm^{-1}, which corresponds to the nitrate group (in Fig. S1). As evidenced by its infrared absorption in this strong new band [49], the nitrate is not coordinated with the Ag(I) center. Due to the fact that NO_3 is a nonlinear molecular ion, vibrations that NO_3^-stretching vibrations are present, and these are observed as strong peaks at 1098 and 910 cm^{-1} (pure modes; their TED contribution is about 15%).

Based on experiments, the Ag-N (or Ag-pyridine) stretching mode should be given 645,137, 90, and 76 cm^{-1} bands. These experimentally observed values are in agreement with the theory.

Experimentally, 645,137, 90, and 76 cm^{-1} bands should be assigned to the Ag-N (or Ag-pyridine) stretching mode. Also, absorption bands in the range of C-N-Ag bending modes are observed in the range of 120–100 cm^{-1} [50]. This peak is observed at 121 cm^{-1} in the experimental IR of the complex, while 120 cm^{-1} is calculated.

4.3. Non-covalent interactions

4.3.1. Topological analysis (AIM)

The AIM (Atoms-in-Molecules) analysis enables us to gain a better understanding of the non-covalent interactions occurring inside a molecular system and the strength of hydrogen bonds by examining their topological and energetic characteristics [51]. Fig. 3 shows the AIM topology graph of the Ag(I) complex. Also, the bond critical point (BCP) for this system was clearly marked. There is a potential for hydrogen bond interaction between C-H....O in the complex, as seen in Fig. 3. The topological parameters of non-covalent interactions are given in Table 1. The calculated values of the electron density ρ(r), the Laplacian of the electron density $\nabla^2\rho(r)$, the eigenvalues of the Hessian matrix (λ_1, λ_2, λ_3), density total energy H(r), Lagrangian kinetic energy G(r), local electron potential V(r) and bond energy (E_{bond} = V(r)/2), in Table 1. The AIM results showed that the Ag(I) complex is characterized by four BCPs, which define the C-H...O type interaction. According to Rozas et al. [52], these hydrogen bonds are strong hydrogen bonds if the electron density is $\nabla^2\rho(r) < 0$ and the total energy density is H (r) < 0; If $\nabla^2\rho(r) > 0$ and H(r) >0 it is considered a weak hydrogen bond. According to the results, the Laplacian of charge density values are positive, indicating that the electronic charge is depleted along the binding pathway and the presence of ionic interaction [53]. The calculated interaction energy at BCP indicates that in the interactions between C_{34}-H_{40}....O_{57} in complex has the highest value of interaction energy, so it is the strongest interaction.

Based on the results of the QTAIM analysis of the Ag-N appearing in the molecular graph of the complex. For the Ag-N_3, Ag-N_{22} and Ag-N_{29} bonds, $\nabla^2\rho$(r) is positive and H(r) is negative, indicating that the bond is partially covalent character. The positive values of $\nabla^2\rho$(r) and H(r) for Ag-N_{14} indicate that the bond has an electrostatic character.

4.3.2. Reduced gradient of density (RDG)

The non-covalent interactions (NCI) approach may be used to investigate all forms of interactions, especially in low-density areas or regions [54]. As can be seen in the predicted RDG plot, there are three areas of interaction. Regions marked in green indicate Van der Waals interactions, the red color corresponds to repulsive interactions (steric effect) localized mainly at the loop level, while the blue color indicates the presence of hydrogen bonds. The predicted RDG plot for the Ag(I) complex is given in Fig. 4. Looking at the graphs, the red region indicates strong repulsive interactions mainly observed in the centers of the pyridine ring (steric effect), the blue color represents C-H...O strong hydrogen bond interactions, while the green sign represents strong repulsion and interactions region Van der Waals (VDW) interactions. The green regions of interactions corresponding to the VDW have a very high density of complex structure due to H.....H interactions.

4.3.3. ELF and LOL analyses

Topology analysis of the electron localization function (ELF), and localized orbital locator (LOL) is often employed to show atomic

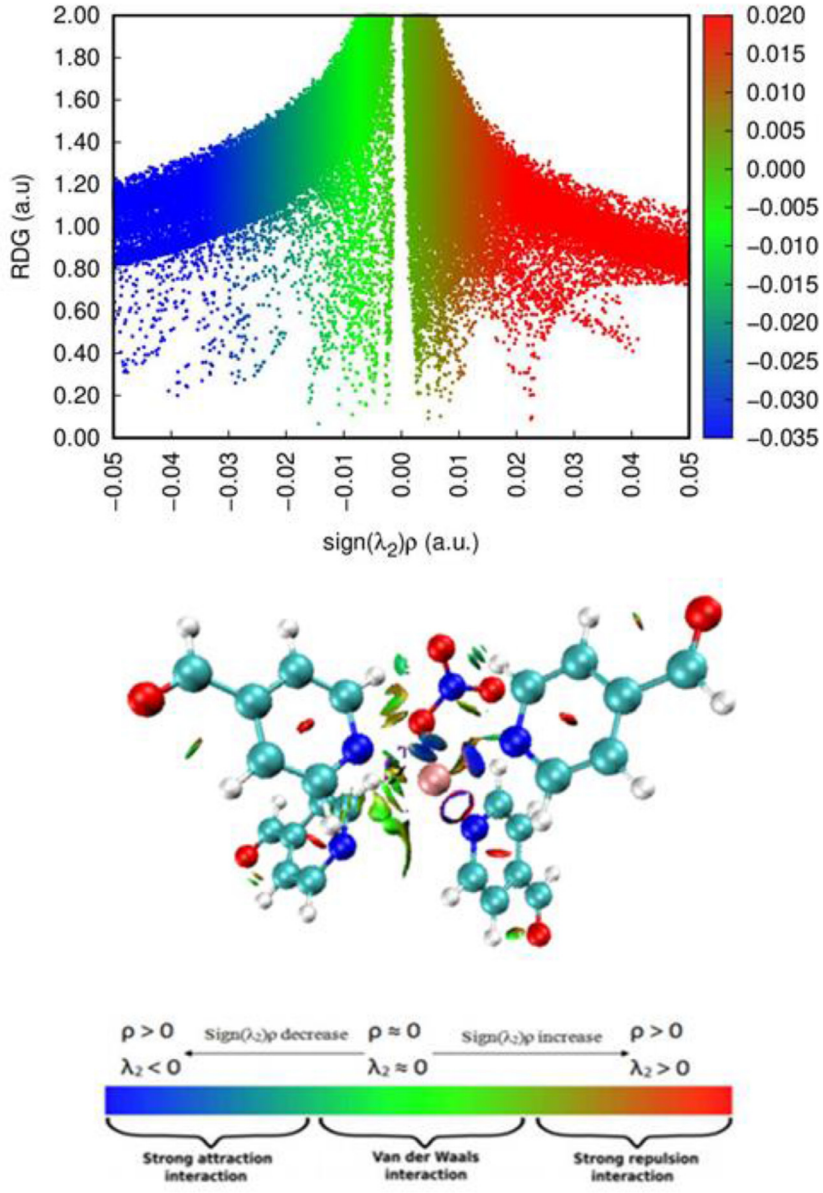

Fig. 4. 2D scatter and Isosurface density plots illustrating the non-bonded interactions of $[Ag(4\text{-}PCA)_4]NO_3$.

shell structure, chemical bonding classification, and charge-shift bond verification on the molecular surface. The electron environment of each atom is characterized by a relief map with a large or contracted peak region. These results show how easy it is to discover an electron pair on a molecular surface [2]. ELF and LOL have a chemical relationship that is comparable in that they both rely on the density of kinetic energy. While ELF is due to the density of the electron pair, LOL only shows the gradient of localized orbitals and is used when localized orbitals overlap [55]. LOL expresses much more stable and vivid depictions than ELF. 2D and 3D depictions of the ELF and LOL isosurface for the Ag (I) complex in Fig. 5. The Fig. 5(a) shows, the highly localized bond and non-bond electrons around hydrogen atoms, which are shown by elevated ELF regions. The electron cloud delocalized around some carbon atoms (C1, C2, C15, C17, C26, C27, C33, C34) is represented by blue regions. The electron depletion region where electrons are highly localized (red region) around H13, and H48 hydrogen atoms is shown in the ELF map. The blue circle around oxygen atoms O37 and O51 is the region of electronic depletion between the inner layer and the valance layer. The region with red and orange colors represents a strong electronic localization. In this region, there are oxygen atoms in the complex. The covalent bond exists around carbon-carbon atoms, as evidenced by the red color and high LOL value. In Fig. 5(b), the white color in the central region of the H13 hydrogen atom denotes the crossing of the color scale limit in the form of electron density.

4.3.4. Natural bond orbital (NBO) study

The natural bonding orbital (NBO) study is used to evaluate the inter and intra molecule H-bonding interactions of various chemical systems [56,57]. Also, the NBO analysis provides a suitable foundation for examining the high electron density in the molecular system's orbital bonding [58]. The interaction between donor and acceptor is characterized by significant energy $E^{(2)}$ in the NBO analysis [51]. Table 2 selects interactions with stabilization energies $E^{(2)} > 5$ kcal/mol. The most important interaction of energy in the titled complex was the electron coupling $\pi^*(N_{14} - C_{15}) \rightarrow \pi^*(C_{16} - C_{17})$, $\pi^*(C_2 - N_3) \rightarrow \pi^*(C_1 - C_6)$, $\pi^*(N_{29} - C_{34}) \rightarrow \pi^*(C_{30} - C_{31})$, which

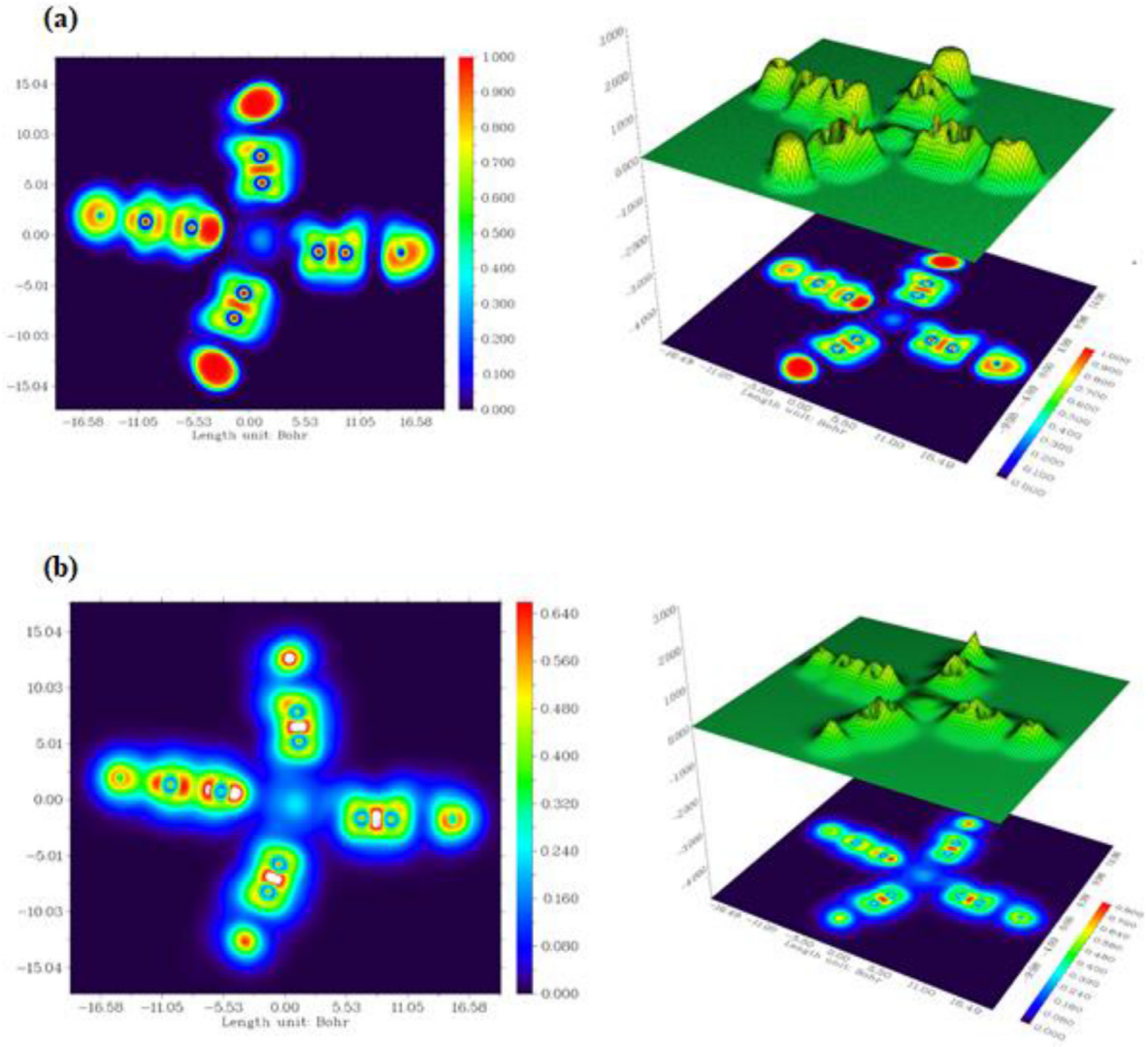

Fig. 5. Relif map and Color filled map of (a) ELF and (b) LOL of $[Ag(4\text{-}PCA)_4]NO_3$.

stabilizes at 194.87, 132.32 and 132.85 kcal/mol respectively. The outcome of the second perturbation theory highlights the fact that electron transfer from the N-C and the C-C in the pyridine ring is predominant.

The biological activity of a molecule is defined by the stabilizing interactions between the LP orbitals and the σ^* or π^* orbitals. [59]. The stabilization energy of LP(O), and LP(C) donors that interact with neighboring antibonding acceptors $\pi^*(N_{54} - O_{56})$, $\sigma^*(N_{54} - O_{56})$ and $\pi^*(N_{29} - C_{34})$, $\pi^*(C_{30} - C_{31})$ is computed in this work, with the energies of 108.61, 83.39, and 101.06, 59.82 kcal/mol for the Ag(I) complex. The biological activity of the title compound is therefore validated based on the nbo results.

The chemical interpretation of hyperconjugation interactions and Electron Density Transfer from the filled lone electron pair n(Y) to Lewis base Y into the unfilled antibond $\sigma^*(X - H)$, of the "Lewis acid" X-H in the X-H...Y hydrogen bond system is also provided by the NBO analysis [60,61]. Intermolecular C-H....O hydrogen bonding is generated in complexes by orbital overlap between the oxygen (O) lone electron pair and the $\sigma^*(C - H)$ antibonding orbitals, which results in intermolecular charge transfer and causes stabilization of H-bonded systems. The magnitude of charge transfer from lone pair $LP(2)O_{57}$ to $\sigma^*(C_{27} - H_{36})$, $LP(1)O_{56}$ to $\sigma^*(C_2 - H_{10})$ and $LP(1)O_{55}$ to $\sigma^*(C_{15} - H_{42})$ with E(2) energies of 3.64, 2.61, and 1.31 kJ/mol, respectively, denotes the extent of the intermolecular hydrogen bond. This is further supported by AIM analysis as well.

4.4. Electronic properties

4.4.1. Frontier molecular orbital and chemical descriptors studies

The highest occupied molecular orbital (HOMO) and the lowest unoccupied molecular orbital (LUMO) can reveal some structural, and physical characteristics as well as the nature of reactivity. Furthermore, the Frontier molecular orbital (FMO) provides interactions in molecules, which are critical in biological properties [62]. Fig. 6 depicts the HOMO-LUMO orbitals of the Ag(I) complex. HOMO stated that the charge density was localized to the nitrate ion and around the metal, and LUMO exhibited unoccupied orbitals that were delocalized to the 4-PCA ligands containing N3, and N22 nitrogen atoms in the pyridine ring.

Chemical reactivity descriptors based on Conceptual Density Functional Theory, such as electronegativity (χ), chemical hardness (η), chemical softness (S), electrophilicity index (ω) and chemical potential (μ), were established to get a better understanding of the compound's chemical reactivity [63]. Table 3 summarizes the reactivity descriptions. The energy gap for the title molecule

Table 2
The second order perturbation energies $E^{(2)}$ (kcal/mol) corresponding to the most important charge transfer interactions (donor–acceptor) in the compound studied by B3LYP/LANL2DZ method.

Donor NBO (i)	*Acceptor NBO (j)*	$E^{(2)}(kcal/mol)^a$	$\varepsilon_j - \varepsilon_i(a.u.)^b$	$F(i,\ j)(a.u.)^c$
$\sigma(C_1 - C_6)$	$\sigma^*(C_2 - N_3)$	27.90	0.25	0.075
	$\sigma^*(C_4 - C_5)$	16.67	0.28	0.063
	$\sigma^*(C_7 - O_8)$	17.82	0.26	0.066
$\pi(C_2 - N_3)$	$\pi^*(C_1 - C_6)$	11.77	0.33	0.056
	$\pi^*(C_4 - C_5)$	23.05	0.33	0.078
$\sigma(C_4 - C_5)$	$\sigma^*(C_1 - C_6)$	21.34	0.28	0.070
	$\sigma^*(C_2 - N_3)$	16.90	0.25	0.058
$\sigma(C_7 - O_8)$	$\sigma^*(C_1 - C_6)$	5.65	0.39	0.045
$LP(1)N_3$	$\sigma^*(C_1 - C_2)$	7.15	0.93	0.075
	$\sigma^*(C_4 - C_5)$	7.07	0.94	0.075
$LP(2)O_8$	$\sigma^*(C_6 - C_7)$	15.81	0.69	0.095
	$\sigma^*(C_7 - H_{13})$	19.44	0.63	0.100
$\pi^*(C_2 - N_3)$	$\pi^*(C_1 - C_6)$	132.32	0.03	0.087
	$\pi^*(C_4 - C_5)$	73.77	0.03	0.072
$LP(1)N_3$	$LP^*(6)Ag$	21.20	0.47	0.090
$\pi(N_{14} - C_{15})$	$\pi^*(C_{16} - C_{17})$	13.88	0.31	0.059
	$\pi^*(C_{18} - C_{19})$	23.24	0.31	0.077
$\pi(C_{16} - C_{17})$	$\pi^*(N_{14} - C_{15})$	24.89	0.26	0.072
	$\pi^*(C_{18} - C_{19})$	17.12	0.28	0.064
	$\pi^*(C_{50} - O_{51})$	18.65	0.26	0.067
$\pi(C_{18} - C_{19})$	$\pi^*(N_{14} - C_{15})$	17.60	0.26	0.061
	$\pi^*(C_{16} - C_{17})$	21.14	0.28	0.069
$\pi(C_{50} - O_{51})$	$\pi^*(C_{16} - C_{17})$	5.52	0.39	0.045
$LP(1)O_{51}$	$RY^*(C_{50})$	11.73	1.80	0.130
	$\pi^*(C_{17} - C_{50})$	15.63	0.70	0.094
	$\pi^*(C_{50} - H_{52})$	19.52	0.63	0.100
$\pi^*(N_{14} - C_{15})$	$\pi^*(C_{16} - C_{17})$	194.87	0.02	0.084
	$\pi^*(C_{18} - C_{19})$	112.99	0.02	0.074
$\pi(N_{22} - C_{27})$	$\pi^*(C_{23} - C_{24})$	22.91	0.33	0.078
	$\pi^*(C_{25} - C_{26})$	11.71	0.33	0.056
$\pi(C_{23} - C_{24})$	$\pi^*(N_{22} - C_{27})$	16.96	0.25	0.050
	$\pi^*(C_{25} - C_{26})$	21.37	0.28	0.070
$\pi(C_{25} - C_{26})$	$\pi^*(N_{22} - C_{27})$	27.99	0.25	0.075
	$\pi^*(C_{23} - C_{24})$	16.63	0.28	0.063
	$\pi^*(O_{28} - C_{47})$	117.78	0.26	0.066
$\pi(O_{28} - C_{47})$	$\pi^*(C_{25} - C_{26})$	5.66	0.39	0.045
$LP(2)O_{28}$	$\sigma^*(C_{25} - C_{47})$	15.82	0.69	0.095
	$\sigma^*(C_{47} - H_{48})$	19.45	0.63	0.100
$\pi(N_{22} - C_{27})$	$\pi^*(C_{23} - C_{24})$	70.97	0.03	0.072
	$\pi^*(C_{25} - C_{26})$	129.65	0.03	0.087
$LP(1)N_{22}$	$LP^*(6)Ag$	22.26	0.47	0.092
$\pi(N_{29} - C_{24})$	$LP^*(1)C_{33}$	27.51	0.19	0.078
$\pi(N_{29} - C_{34})$	$\pi^*(C_{30} - C_{31})$	24.97	0.31	0.079
$\pi(C_{30} - C_{31})$	$LP(1)C_{32}$	53.19	0.14	0.093
$LP(1)C_{32}$	$\pi^*(C_{30} - C_{31})$	59.82	0.13	0.100
	$\pi^*(O_{37} - C_{46})$	50.13	0.12	0.096
$LP(1)C_{33}$	$\pi^*(N_{29} - C_{34})$	101.06	0.11	0.115
$LP(1)O_{37}$	$RY^*(C_{46})$	11.74	1.80	0.130
$LP(2)C_{37}$	$\sigma^*(C_{32} - C_{46})$	15.89	0.69	0.095
	$\sigma^*(C_{46} - H_{49})$	19.73	0.62	0.100
$\pi^*(N_{29} - C_{34})$	$\pi^*(C_{30} - C_{31})$	132.85	0.02	0.074
$LP(1)N_{29}$	$LP^*(8)Ag$	12.30	1.27	0.008
$LP(2)O_{55}$	$LP^*(9)Ag$	10.91	0.87	0.087
$LP(3)O_{55}$	$\pi^*(N_{54} - O_{56})$	83.39	0.14	0.107
$LP(2)O_{56}$	$\sigma^*(N_{54} - O_{55})$	13.80	0.55	0.078
	$\sigma^*(N_{54} - O_{57})$	15.27	0.58	0.084
$LP(2)O_{57}$	$\sigma^*(N_{54} - O_{55})$	12.82	0.55	0.075
	$\sigma^*(N_{54} - O_{56})$	14.11	0.59	0.081
$LP(3)O_{57}$	$\sigma^*(N_{54} - O_{56})$	108.61	0.13	0.114

σ : sigma bonds, π : pi bonds, *LP*: lone pairs, RY^* Rydberg.
a $E^{(2)}$ means energy of hyper conjugative interactions.
b Energy difference between donor and acceptor i and j NBO orbitals.
c $F_{(i,j)}$ is the Fock matrix element between i and j NBO orbitals.

is Eg = 3.18 eV in Table. The energy gap represents the molecule's sensitive characteristics and is comparable with many other bioactive compounds [64]. The synthesized compound has a low softness value of 0.31 and a high electrophilic index value of 7.53 (as strong electrophiles with $\omega > 1.5$ eV). The title compound's low softness value suggests that it is less toxic, while its high electrophilic index emphasizes its biological activity [65,66]. In addition, a high electrophilic index value indicates that the likeness of the molecule towards electrons results in better reactivity.

4.4.2. Molecular electrostatic potential (MEP)

The MEP surface is a crucial tool for understanding electrostatic (electron and nuclei) distribution potential and visualizing the reactive site in a wide range of chemical processes, including

Table 3
Calculated energy values of the title compound by B3LYP/6- 311++G(d,p) method.

Energy gap (eV)	Ionization potential (I) (eV)	Electron affinity (A) (eV)	Global hardness (η) (eV)	Electronegativity (χ) (eV)	Chemical potential (μ_c) (eV)	Global softness (σ) $(eV)^{-1}$	Global electrophilicity (ω) $(eV)^{-1}$
3.18	6.52	3.33	1.59	4.93	−4.93	0.31	7.53

H: HOMO, L: LUMO.
$I = -E_{HOMO}$, $A = -E_{LUMO}$, $\eta = \frac{(I-A)}{2}$, $\mu = \frac{-(I+A)}{2}$, $\chi = \frac{(I+A)}{2}$, $\sigma = \frac{1}{2\eta}$, $\omega = \mu^2/2\eta$.

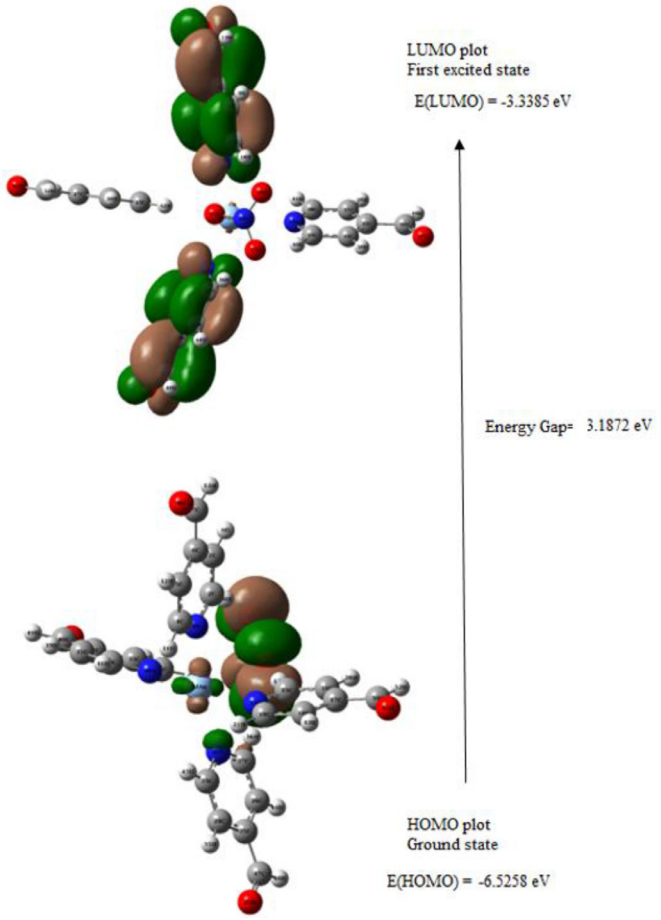

Fig. 6. Frontier molecular orbitals of the title compound.

electrophilic and nucleophilic assaults, and hydrogen bonding interactions [67]. Drug receptor and enzyme substrate interactions are mostly dominated by hydrogen and halogen bonding interactions [68]. Therefore, it is critical in forecasting the reactivity of a chemical to biological systems. The molecular electrostatic potential analysis is beneficial for understanding the charge-related characteristics of the complex's molecular structure. Fig. 7 shows the calculated reactive sites for electrophilic and nucleophilic attack on the title Ag complex. Due to the lone pair electron, which is depicted in red in MEP, the electrophilic attack is essentially localized to the electron-rich oxygen atoms, which is why the strong red colors are observed in the nitrete group. The positive regions (blue color) for nucleophilic attack of the Ag complex are located around the hydrogen atoms attached to the nitrogen and carbon atoms. This means that all hydrogen atoms have the strongest attraction, whereas the oxygen atom has the strongest repulsion.

4.4.3. UV spectral analysis

The UV-vis spectrum of the title Ag(I) complex was determined theoretically in DMSO solvent as well as experimentally in solution using DMSO as the solvent using the TD-DFT method. The experimental and theoretical spectra are shown comparatively in Fig. 8 and the λ_{max} value, excitation energies, oscillator power (f) and corresponding assignments of the state with the maximum absorption wavelengths are given in Table 4. While the maximum absorption value determined experimentally was 322 nm, the λ_{max} values obtained with the TD-DFT method were 305 nm. In the previous study by Ohno et al., the longest wavelength of the 4-PCA ligand measured in hexane solution was 283.3 nm [8]. When compared to the free ligand, this shifted to a longer wavelength, which supports the experimental result and confirms the coordination of 4-PCA to the silver(I) ion [69]. These bands were assignable to the metal to ligand charge transfer (MLCT) transition. The maximum absorption wavelength in the computed absorption spectra corresponds to the electronic transition from HOMO-4 to LUMO and is interpreted as $n \rightarrow \pi*$ character according to molecular orbital contributions.

The Uv-Vis spectra of the silver complex (Fig. 8) show that there is an additional peak near ~450 nm in the theoretical spectra compared with the experimental spectra. This can be due to the limitations of TD-DFT calculations for charge-transfer systems. The other reason behind the additional peak of the calculated spectrum, the influence of the geometry of the complex cannot be neglected either. Theoretical calculations were made using isolated geometry, while the experimental results were obtained for the bulk material. The experimental result includes interactions such as hydrogen bonding in the lattice, van der Waals force, and electrostatic attraction.

4.5. Fukui function

Fukui function is a commonly used functional local density descriptor for the model of chemical reactivity [70]. Nucleophilic and electrophilic attachment prone atomic locations can be detected using Fukui indices. The equivalent condensed or aromatic Fukui functions on the *j*th atom site can be defined as,

$f_j^+ = q_k(N+1) - q_k(N)$ for nucleophilic attack
$f_j^- = q_k(N) - q_k(N-1)$ for electrophilic attack
$f_j^0 = (1/2)\,[\,q_k(N+1) - q_k(N-1)]$ for neutral (radical) attack

In the equations above, q_j denotes whether the atomic charge at the *j*th atomic site is neutral (N), anionic (N + 1), or negative (N-1) [71]. Morell et al. [72] proposed the binary descriptor $\Delta f(r)$given by the equation, which is defined as the difference between nucleophilic and electrophilic Fukui functions,

$$\Delta f(r) = f^+(\vec{r}) - f^-(\vec{r})$$

The dual descriptor $\Delta f(r)$ makes a clear difference between nucleophilic and electrophilic assault at a certain site. When the dual descriptor $\Delta f(r) > 0$, the site is favored for a nucleophilic attack; when the dual descriptor $\Delta f(r) < 0$, the site is favored for an electrophilic attack [59]. According to the condition for dual descriptor the nucleophilic site for in title complex is silver(I) ion, nitrate group and hydrogen atoms are positive values, i.e. $\Delta f(r) > 0$,

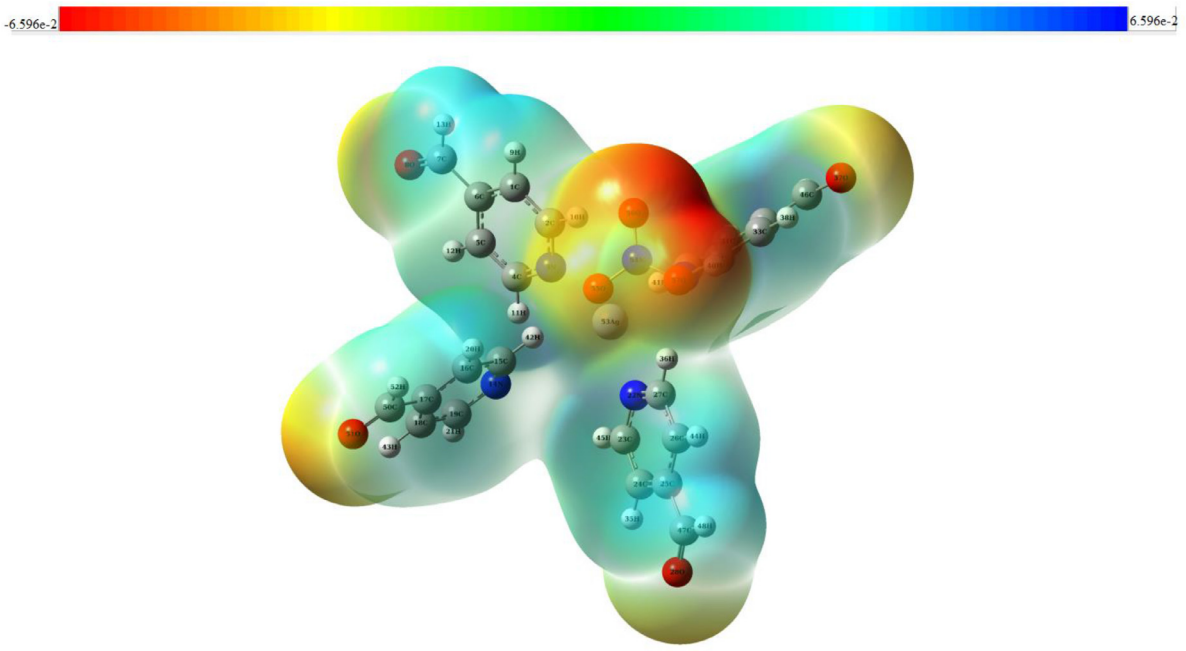

Fig. 7. Molecular electrostatic potential (MEP) maps of $[Ag(4\text{-}PCA)_4]NO_3$.

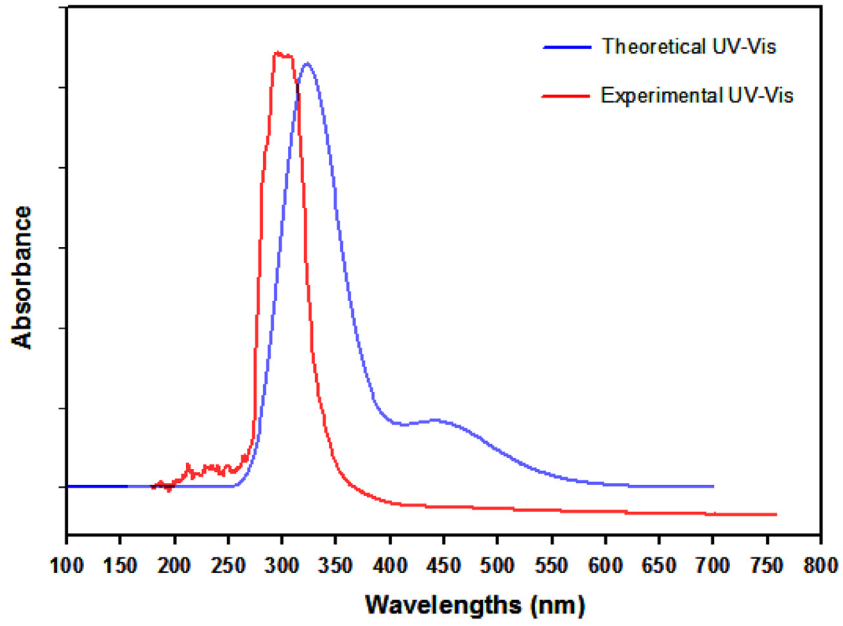

Fig. 8. Comparative UV–vis spectrum of the Ag(I) complex carried out experimentally and theoretically.

Table 4
Experimental and calculated UV-vis wavelength (λ), band gap energy (eV) and oscillator strength for the Ag(I) complex.

HOMO-LUMO Gap	Experimental (DMSO)		TD-DFT/B3LYP/LANL2DZ Solvent phase (DMSO)				
Band Gap (eV)	λ_{max}(nm)	Band Gap (eV)	λ_{max}(nm)	Band Gap (eV)	Osc. Strength (f)	Energy (cm^{-1})	Assignments
3.187	305	4.065	322	3.850	0.1326	47,716	($H_{-4} \rightarrow$ LUMO), ($H_{-3} \rightarrow$ LUMO)

while other atoms are negative values in the electrophilic region, so $\Delta f(r) < 0$. The existence of high electronegativity of the two oxygen atoms, O8 and O28, results in the highest levels of electrophilic nature in C7 and C47. Also, as can be seen from Table S3, carbon, oxygen, and nitrogen atoms have higher electronegativity than hydrogen atoms, rendering hydrogen atoms electron deficient and prone to nucleophilic attack [38].

4.6. Biological evaluation

4.6.1. Molecular docking analysis

Molecular docking allows us to investigate the binding of ligands to proteins, which is particularly useful for screening virtual libraries of drug-like compounds and therefore advancing drug development [63]. Schiff base metal complexes are utilized in

Table 5
Docking parameters of title complex docked with the three protein targets.

Protein (PDB ID)	Bonded residues	No of hydrogen bonds	Bonded distance (Å)	Binding energy (kcal/mol)	Inhibition Constant K_i (μM)	Reference RMSD (Å)
1N5N	SER 64A	5	2.69	−9.27	160.18	82.44
	TRY 88A		2.31			
	TRY 88A		2.55			
	GLY 91A		1.75			
	GLY 97A		1.84			
1LQW	SER 57A	7	1.99	−10.07	41.52	41.32
	VAL 59A		3.02			
	GLN 65A		1.96			
	GLN 65A		3.05			
	THR 107A		2.25			
	LEU 112A		2.53			
	TYR 147A		2.25			
3QP6	MET 72A	5	2.82	−9.11	211.54	52.79
	ASN 77A		2.16			
	ASN 86A		2.37			
	ASN 92A		3.02			
	ALA 94A		2.04			

bioorganometallic chemistry and have a wide variety of biological actions in the treatment of many illnesses. Moreover, silver (Ag), an elemental metal with antibacterial action against a wide range of bacteria, fungi, and viruses, is used in clinical practice because it is effective at low dosages against a wide range of microorganisms. In the present study, the activities of the synthesized molecules for protein selection were analyzed, and then strong activities were taken into account for protein selection. In our antibacterial investigation, the synthesized molecular structure demonstrated good antibacterial efficacy against Gram-positive and Gram-negative bacteria. Hence, we decided to perform the docking procedure for the title Ag(I) complex structure with antimicrobial and antiquorum-sensing activity receptor proteins such as *Pseudomonas aeruginosa* (PDB ID: 1N5N); *Staphylococcus aureus* (PDB ID: 1LQW); *Chromobacterium violaceum* (PDB ID: 3QP6). The target proteins' crystal structures were taken from the RCSB database (www.pdb.org). As shown in Table 5, the docking parameters, calculated inhibition constant, binding energy, and hydrogen bond distance, all play a role in determining the type of the molecule. The binding interactions of the Ag(I) complex with three protein targets are depicted in Fig. 9. From the docking results in Table 5 and Fig. 9, the molecule and 1LQW (receptor) have binding energy and inhibition constant values of −10.07 Kcal/mol and 41. 52 μM. Similarly, other proteins, 1N5N and 3QP6, form a hydrogen bond with a complex with binding energy of −9.27 and −9.11 Kcal/mol. All proteins, the hydrogen bonded amino acid bond lengths of < 3 Å which indicates that they are all strong hydrogen bonding interactions. The biological activity of the title compound is confirmed by the docking of all three proteins with the Ag(I) complex. Furthermore, the protein targets under consideration, the titled compound, show the best pharmacological activity against 1LQW with lower binding energies and Ki values. These results reveal that the synthesized complex structure can act as a potential antibacterial agent.

4.6.2. In silico *ADMET and toxicity predictions*

Because of their precision, speed, and accessibility, computational-based in-silico toxicity measurements have become popular. They may give information on any synthetic or natural chemical. Pro-Tox II [31] was used to estimate the ligands' organ toxicity, toxicological endpoints, and median lethal dose (LD_{50}). ADMET is a crucial metric for determining a compound's fate when taken orally. The computed results in SwissADME [30] and Pre-ADMET software [29], Pro-Tox II of the silver complex are given in Tables 6 and 7. According to the SwissADME estimate criteria, the title chemical exhibited high gastrointestinal (GI) absorption, but no blood-brain barrier (BBB) penetration. The lack of blood brain barrier (BBB) permeation is a desired quality based on the location of the target, where unnecessary permeation should be avoided [73]. Caco-2 (colorectal carcinoma) cell permeability values showed poor permeability (< 25 poor, > 500 great; standard range). The results of human intestine absorption (HIA) suggest that the Ag(I) complex could be absorbed from the intestine into the bloodstream by 81%. Plasma protein binding (PPB) affects how long a medication stays in the body and can potentially impact its effectiveness. The level of plasma protein binding has an important effect on the pharmacological and pharmacokinetic behavior of the medication. The observed 100% PPB value for the compound indicates a strong (effectively) binding ability to plasma protein. The skin permeability, Kp, value (10.14% cm/h) falls within the standard range of low skin permeability (−8.0 to −10 cm/h). The lower negative value of log Kp leads to less permeability of the compound. Acute toxicity prediction findings, such as toxicity class classification [1 (toxic) to 6 (non-toxic), indicated that the named chemical was classified as acute toxicity class 4 (harmful if swallowed). According to the ProTox-II server, the predicted LD_{50} value of the compound is 640 mg/kg and the results suggest that the compound is non-carcinogenic in complex and has no effect on immunotoxicity, cytotoxicity, but has some mutagenicity.

4.6.3. Antibacterial and antiquorum-sensing screening activity

Results of antibacterial activity of all compounds with Minimal Inhibitory Concentration (MIC) and inhibition zone diameter (mm) are shown in Table 8. In the MIC (1000 μg/ml) evaluation in this table, title complex showed good antibacterial activity against all test bacteria (MIC: 3.91–62.5 μg / mL) except *B. cereus.*

In antibacterial activity testing with agar well diffusion, Gram negative bacteria (*E. coli* and *P. aeruginosa*) showed good sensitivity to $4PCAAgNO_3$ when dilued in DMSO (10 mg/ml), and showed mean values of 12.2 and 20.3 mm inhibition zone diameters, respectively (Table 8).

In the agar well diffusion test, $4\text{-}PCAAgNO_3$ showed highly antibacterial activity against the Gram positive bacteria *S. aureus* (DIZ: 15.4 mm) and *S. epidermidis* (DIZ: 15.2 mm) in the agar.

Results were compared with those of standard drug, ampicillin.

The bacterial activity was performed in triplicate and the mean inhibitory zones were recorded**.** Victoria et al. [74] reported inhibition zones as DIZ > 15 mm = highly active, DIZ > 10 mm = moderately active, DIZ > 5 mm = slightly active, and DIZ ≤ 5 mm = inactive, respectively.

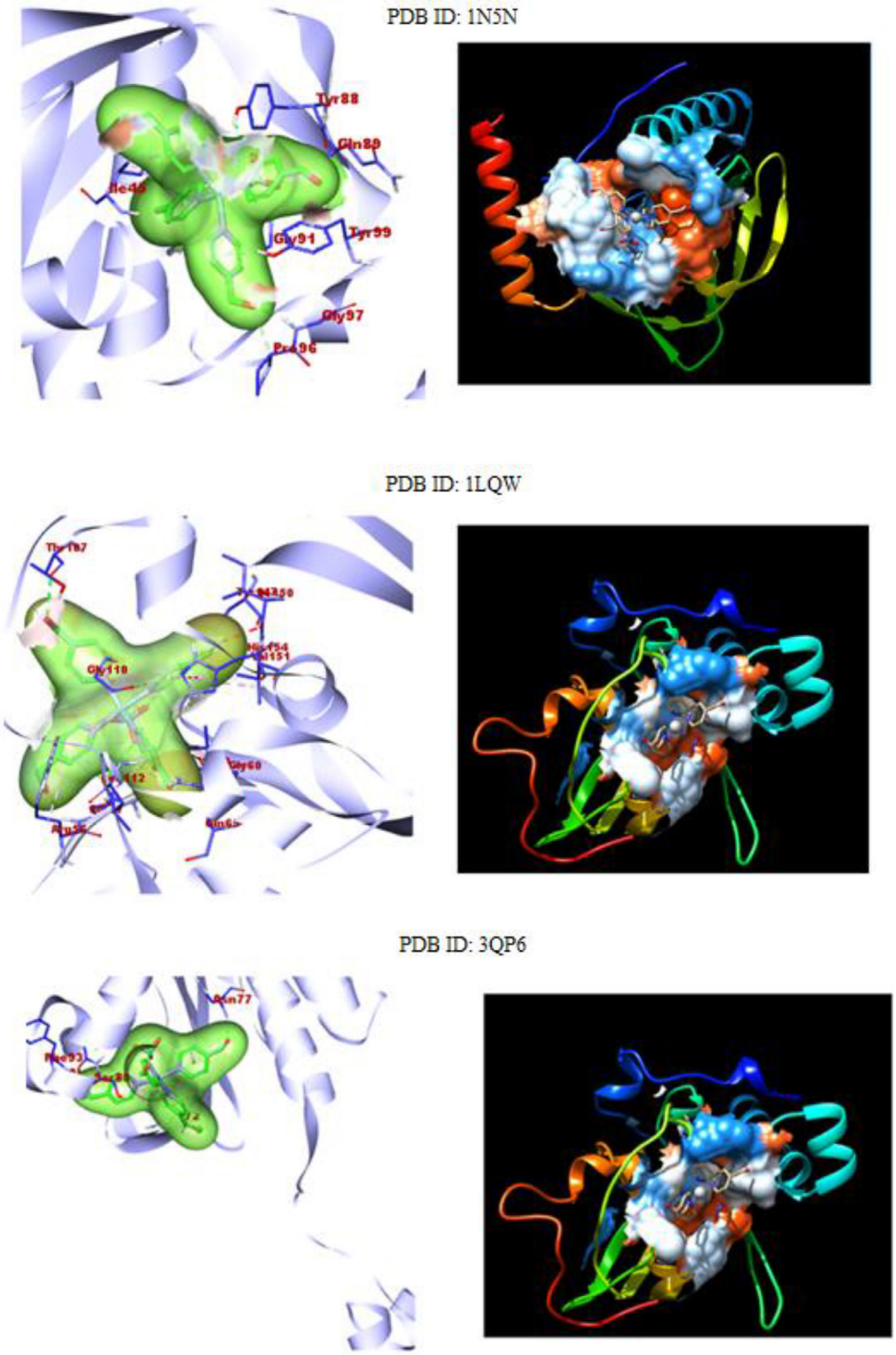

Fig. 9. 3D bonding between amino acid residue and $[Ag(4\text{-}PCA)_4]NO_3$ complex.

Table 6
ADME predictions of Ag(I) complex, computed by SwissADME and PreADMET.

Compound	GI absorption	BBB	Caco2 permeability	HIA	Bioavailability Score	Log Kp	PPB
$[Ag(4PCA)_4NO3]$	High	No	10.76		81.10 0.17	−10.48	100

Log Kp: skin permeation value; GI: gastro-intestinal; BBB: blood–brain barrier; PPB: Plasma protein binding; HIA: Human Intestinal Absorption.

Table 7
Toxicity predictions of Ag(I) complex calculated by Pro-Tox II.

Compound	Toxicity LD_{50} (mg/kg) Class	Organ Toxicity Hepatotoxicity	Carcinogenicity	Immunotoxicity	Mutagenicity	Cytotoxicity
$[Ag(4PCA)_4NO3]$ 4	640		Inactive	Inactive	Inactive	Active Inactive

Table 8
Antibacterial activity results of silver(I) complex by Minimum Inhibitory Concentration (MIC) and the inhibition zone diameter (mm).

Test Bacteria	DIZ (mm)	MIC (µg/ml)	AMP (10 µg)	10%DMSO
S. aureus ATCC 29,213	15.4	7.81	18	–
S. epidermidis ATCC 35,984	15.2	3.91	16	–
L.monocytogenes ATCC 35,152	13.2	7.81	15	–
B. subtilis ATCC 6633	8.0	62.5	12	–
B. cereus 709 Roma	–	–	12	–
E. faecalis ATCC 29,212	8.0	62.5	18	–
E. coli ATCC 25,922	12.2	3.9	18	–
S.typhimurium ATCC 14,028	10.3	31.25	16	–
P. aeruginosa ATCC 27,853	20.3	7.81	16	–
K. pneumoniae ATCC 13,883	10.2	31.25	15	–
C. violaceum ATCC12472 (Antiquorum-sensing activities)	15	–	–	–

MIC (µg/ml): Minimum Inhibitory Concentration.
DIZ (mm)**:** Diameter of inhibition zone (mm).
Positive control: AMP (10 µg): Ampicillin.
Negative control: 10% DMSO.
Note: – indicates no inhibition.

Microbial quorum-sensing systems (QS), focus on regulating microbial resistance mechanisms and regulation of microbial biofilm formation, and a new strategy can be developed for the treatment of proposed drug resistant bacteria using QS to prevent microbial resistance [75]. *C. violaceum,* produces purple pigment violacein, the production of which is regulated by acyl homoserine lactones (AHLs) -mediated QS.

Thus, drugs that inhibit acyl HSL-mediated QS activity in *C. violaceum* will prevent the production of this purple pigment [76]. Screening results (based on measurement of pigment inhibition radius in mm) for their ability to inhibit the production of violaceum regulated by QS against *C. violaceum* are presented in Table 8 and show that compound 4-PCA$AgNO_3$ has potent antiquorum sensing activity.

5. Conclusion

In the present work, we report a detailed investigation of a newly synthesized silver(I) complex. Reduced density gradient analysis of C-H...O bonds as noncovalent interactions with respect to van der Waals and steric interactions has been demonstrated to be consistent with AIM and NBO results. The electron localization and delocalization centers are clearly predicted by the color-filled ELF map and the contour map of LOL. The HOMO-LUMO energy gap value is an important feature for determining the bioactivity of the title complex. The Uv–Vis spectrum reveals that the compound is transparent in the visible region and that it agrees well with experimental and theoretical values. As a result, the Ag(I) complex showed bacteriocidal activity against test bacteria. Therefore, we propose that the Ag(I) complex can help to design new synthetic antibiotics and disinfectants. The molecular docking study shows excellent interaction score values in agreement with most active compounds. According to *in silico* ADME analyses, this molecule has a good pharmacokinetic profile.

Declaration of Competing Interest

The authors declare that they have no known competing financial interests or personal relationships that could have appeared to influence the work reported in this paper.

CRediT authorship contribution statement

Sibel Celik: Conceptualization, Data curation, Investigation, Methodology, Software, Supervision, Validation, Visualization, Writing – original draft. **Senay Yurdakul:** Conceptualization, Data curation, Methodology, Supervision, Validation, Writing – original draft. **Belgin Erdem:** Conceptualization, Data curation, Methodology, Validation, Writing – review & editing.

References

[1] A. Crespi, V.M.S. ‘ anchez, D. Vega, A.L. Perez, C.D. Brondino, Y.G. Linck, P. Hodgkinson, E. Rodr´ıguez-Castellon´, J.M. Lazaro-Mart ‘ınez, Paramagnetic solid-state NMR assignment and novel chemical conversion of the aldehyde group to dihydrogen ortho ester and hemiacetal moieties in copper(II) and cobalt(II)-pyridinecarboxaldehyde complexes, RSC Adv. 11 (2021) 20216–20231.
[2] K. Arulaabaranama, G. Mani, S. Muthu, omputational assessment on wave function (ELF, LOL) analysis, molecular confirmation and molecular docking explores on 2-(5-Amino-2- Methylanilino)-4-(3-pyridyl) pyrimidine, Chem. Data Collect. 29 (2020) 100525.
[3] P.V. Rao, G.S. Prasad, P.S.S. Prasad, Novel synthesis, characterization and biologicalStudies of Schiff base complexes of 4-pyridine Carboxaldehyde, Int. J. Pharma. Dev. Tech. 4 (2014) 245–248.
[4] T.S.H. Korich, A. Facile, One-pot procedure for forming diarylimines from nitroarenes and benzaldehydes, Synlett 16 (2007) 2602–2604.
[5] K.L.P.S. Lovely, M. Christudhas, The DNA cleavage and antimicrobial studies of Co(II), Ni(II), Cu(II) and Zn(II) complexes of 4-pyridinecarboxaldehyde with 4-aminopyridine, IOSR J. Appl. Chem. 4 (2013) 14–19.
[6] A.D. Russell, W.B. Hugo, Antimicrobial activity and action of silver, Prog. Med. Chem. 31 (1994) 351–370.
[7] E. Hidalgo, R. Bartolome, C. Barroso, et al., Silver nitrate: antimicrobial activity related to cytotoxicity in cultured human fibroblasts, Skin Pharmacol. Appl. Skin Physiol. 11 (1998) 140–151.
[8] A.B.G. Lansdown, Silver I: its antibacterial properties mechanism of action, J. Wound Care 11 (2002) 125–130.
[9] A. Kedziora, M. Speruda, E. Krzyzewska, J. Rybka, A. Łukowiak, G. Bugla-Płoskońska, Similarities and differences between silver ions and silver in nanoforms as antibacterial agents, Int. J. Mol. Sci. 19 (2018) 444.
[10] M. Baia, L. Baia, W. Kiefer, J. Popp, Surface-enhanced raman scattering and density functional theoretical study of anthranil adsorbed on colloidal silver particles, J. Phys. Chem. B 108 (2004) 17491–17496.
[11] S. Günal, N. Kaloglu, I. Ozdemir, S. Demir, I. Ozdemir, Novel benzimidazolium salts and their silver complexes: synthesis and antibacterial properties, Inorg. Chem. Commun. 21 (2012) 142–146.
[12] A. Panacek, L. Kvitek, R. Prucek, M. Kolar, R. Vecerova, N. Pizurova, V.K. Sharma, T.j. Nevecn, R. Zboril, Silver colloid nanoparticles: synthesis, characterization, and their antibacterial activity, J. Phys. Chem. B 110 (2006) 16248–16253.

[13] B. Thati, A. Noble, R. Rowan, B.S. Creaven, M. Walsh, M. McCann, D. Egan, K. Kavanagh, Mechanism of action of coumarin and silver (I)–coumarin complexes against the pathogenic yeast Candida albicans, Toxicol. In Vitro 21 (2007) 801–808.

[14] B.S. Creaven, D.A. Egan, K. Kavanagh, M. McCann, M. Mahon, A. Noble, B. Thati, M. Walsh, Synthesis and antimicrobial activity of copper(II) and silver(I) complexes of hydroxynitrocoumarins: x-ray crystal structures of [Cu(hnc)2(H2O)2] • 2H2O and [Ag(hnc)] (hncH = 4-hydroxy-3-nitro-2H-chromen-2-one), Polyhedron 24 (2005) 949–957.

[15] K.L.P. Sheeja Lovely, M. Christudhas, he DNA cleavage and antimicrobial studies of Co(II), Ni(II), Cu(II) and Zn(II) complexes of 4-pyridinecarboxaldehyde with 4-aminopyridine, IOSR J. Appl. Chem. (IOSR-JAC) 4 (2013) 14–19.

[16] E.M. Njogu, B. Omondi, V.T.O. Nyamori, Silver(I)-pyridinyl Schiff base complexes: synthesis, characterisation and antimicrobial studies, J. Mol. Struct. 1135 (2017) 118–128.

[17] NCCLS, 2000. Performance Standards for Antimicrobial Susceptibility Testing: 10th Informational Supplement (Aerobic Dilution, MIC Testing Supplemental Tables. NCCLS document M100-S10(M7), supplement to NCCLS document M7-A5 (MIC testing).

[18] NCCLS 2003, Performance Standards for Antimicrobial Susceptibility Testing:13th Informational Supplement (Disk Diffusion Supplemental Tables). NCCLS document M100-S13 (M2), supplement to NCCLS document M2-A8 (disk diffusion).

[19] M.J. Frisch, G.W. Trucks, H.B. Schlegel, G.E. Scuseria, M.A. Robb, J.R. Cheeseman, G. Scalmani, V. Barone, B. Mennucci, G.A. Petersson, H. Nakatsuji, M. Caricato, X. Li, H.P. Hratchian, A.F. Izmaylov, J. Bloino, G. Zheng, J.L. Sonnenberg, M. Hada, M. Ehara, K. Toyota, R. Fukuda, J. Hasegawa, M. Ishida, T. Nakajima, Y. Honda, O. Kitao, H. Nakai, T. Vreven, J.A. Montgomery Jr., J.E. Peralta, F. Ogliaro, M. Bearpark, J.J. Heyd, E. Brothers, K.N. Kudin, V.N. Staroverov, R. Kobayashi, J. Normand, K. Raghavachari, A. Rendell, J.C. Burant, S.S. Iyengar, J. Tomasi, M. Cossi, N. Rega, J.M. Millam, M. Klene, J.E. Knox, J.B. Cross, V. Bakken, C. Adamo, J. Jaramillo, R. Gomperts, R.E. Stratmann, O. Yazyev, A.J. Austin, R. Cammi, C. Pomelli, J.W. Ochterski, R.L. Martin, K. Morokuma, V.G. Zakrzewski, G.A. Voth, P. Salvador, J.J. Dannenberg, S. Dapprich, A.D. Daniels, Ö. Farkas, J.B. Foresman, J.V. Ortiz, J. Cioslowski, D.J. Fox, Gaussian 09, Gaussian, Inc., Wallingford CT, 2009.

[20] R. Dennington II, T. Keith, J. Millam, GaussView, Version 5, Semichem, Shawnee Mission, KS, 2009.

[21] T. Lu, F. Chen, Multiwfn: a multifunctional wavefunction analyzer, J. Comput. Chem. 33 (2012) 580–592.

[22] W. Humphrey, A. Dalke, K. Schulten, VMD: visual molecular dynamics, J. Mol. Graph. 14 (1996) 33–38.

[23] T. Lu, F. Chen, Multiwfn: a multifunctional wavefunction analyzer, J. Comput. Chem. 33 (2012) 580–592.

[24] T. Lu, F. Chen, Quantitative analysis of molecular surface based on improved marching tetrahedra algorithm, J. Mol. Graph. Model. 38 (2012) 314–323.

[25] E. Runge, E.K.U. Gross, Density-functional theory for time-dependent systems, Phys. Rev. Lett. 52 (1984) 997–1000.

[26] G.M. Morris, D.S. Goodwill, R.S. Halliday, R. Huey, W. Hart, R.K. Belew, A.J. Olson, Automated docking using a Lamarckian genetic algorithm and an empirical binding free energy function, J. Comput. Chem. 19 (1998) 1639–1662.

[27] T.D. Goddard, C.C. Huang, T.E. Ferrin, Visualizing density maps with UCSF Chimera, J. Struct. Biol. 157 (1) (2007) 281–287 Jan[Medline: 16963278], doi:10.1016/j.jsb.2006.06.010.

[28] Dassault Systèmes BIOVIA, Discovery Studio Modeling Environment, Release 2017, San Diego: Dassault Systèmes, 2016.

[29] Available at: www.preadmet.com

[30] Available at: www.swissadme.ch/index.php.

[31] Available at: http://tox.charite.de/protox_II/

[32] G.F. Swiegers, T.J. Malefetse, New self-assembled structural motifs in coordination chemistry, Chem. Rev. 100 (2000) 3483–3538.

[33] I. Yılmaz, N. Acar-Selçuki, S.J. Coles, F. Pekdemir, A. Sengül, Spectroscopic, structural and DFT studies of luminescent Pt(II) and Ag(I) complexes with an asymmetric 2,2-bipyridine chelating ligand, J. Mol.Struct. 1223 (2021) 129271.

[34] I.L. Paiva, G.S.G. de Carvalho, A.D. da Silva, P.P. Corbi, et al., Silver(I) complexes with symmetrical Schiff bases: synthesis, structural characterization, DFT studies and antimycobacterial assays, Polyhedron 62 (2013) 104–109.

[35] F. Tuna, J. Hamblin, G. Clarkson, W. Errington, N.W. Alcock, M.J. Hannon, Helical (isotactic) and syndiotactic silver(I) metallo-supramolecular coordination polymers assembled from a readily prepared bis-pyridylimine ligand containing a 1,5-naphthalene spacer, Chem. A Eur. J. 8 (2002) 4957–4964.

[36] A.R. Biju, M.V. Rajasekharan, Unusual coordination geometries of silver(I) 4,5-diazafluoren-9-one complexes, Polyhedron 27 (2008) 2065–2068.

[37] S.M. Solimana, A. Barakat, Self-assembly of azine-based hydrolysis of pyridine and isatin oxamohydrazides with $AgNO_3$; synthesis and structural studies of a novel four coordinated Ag(I)-azine 2D coordination polymer, Inorg. Chim. Acta 490 (2019) 227–234.

[38] J.D. Deephlin Tarika, X.D. Divya Dexlin, S. Madhankumar, D.D. Jayanthi, T.J. Beaula, Tuning the computational evaluation of spectroscopic, ELF, LOL, NCI analysis and molecular docking of novel anti COVID-19 molecule 4-dimethylamino pyridinium 3, 5-dichlorosalicylate, Spectrochim. Acta Part A 259 (2021) 119907.

[39] H.M. Robert, D. Usha, M. Amalanathan, R. Racil JeyaGeetha, M.S.M. Mary, Spectroscopic (IR, Raman, UV, NMR) characterization and investigation of reactive properties of pyrazine-2-carboxamide by anti-bacterial, anti-mycobacterial, Fukui function, molecular docking and DFT calculations, Chem. Data Collect. 30 (2020) 100583.

[40] L. Cluyts, A. Sharma, N. Kuş, K. Schoone, R. Fausto, Matrix isolation infrared spectroscopic study of 4-Pyridinecarboxaldehyde and of its UV-induced photochemistry, Spectrochim. Acta Part A 171 (2017) 207–212.

[41] V. Krishnakumar, R.J xavier, Normal coordinate analysis of vibrational spectra of 2-methylindoline and 5-hydroxyindane, Indian J. Pure Appl. Phys. 41 (2003) 95–98.

[42] R.M. Silverstein, F.X. Webster, Spectrometric Identification of Organic Compounds, 6th ed., John Wiley Inc, New york, 2003.

[43] [.D.N. Sathyanarayanan, Vibrational Spectroscopy Theory and Applications, 1st ed., New Age International, New Delhi, 2000 Published by.

[44] G. Varsainyi, Assignments Vib. Spectra Seven Hundred Benzene Deriv, Wiley: New York, 1974.

[45] H. M.Robert, D. Usha, M. Amalanathan, R.R.J. Geetha, M.S. M.Mary, Vibrational spectral, density functional theory and molecular docking analysis on 4-nitrobenzohydrazide, J. Mol. Struct. 1223 (2021) 128948.

[46] K.R. Santhy, M. Daniel Sweetlin, S. Muthu d, C.S. Abraham, M. Raja, Molecular structure, spectroscopic (FT-IR, FT-Raman) studies, Homo–Lumo and Fukui function calculations of 2-Acetyl amino-5-bromo- 4 methyl pyridine by density functional theory, Chem. Data Collect. 24 (2019) 100291.

[47] S.S. Margreat, S. Ramalingam, S. Sebastian, S. Xavier, S. Periandy, J.C. Daniel, M.M. Julie, DFT, spectroscopic, DSC/TGA, electronic, biological and molecular docking investigation of 2,5-thiophenedicarboxylic acid: a promising anticancer agent, J. Mol. Struct. 1200 (2020) 127099.

[48] J. Junior, M. Cavicchioli, R.T.A. Machado, F. Rogério Pavan, D. Nakahata, P.P. Corbi, et al., Synthesıs, characterızatıon, dft modelıng and ın vıtro antımycobacterıal actıvıty assays of a sılver(ı)-ısonıazıd complex, Quim. Nova 44 (2021) 278–283.

[49] E. Movahedi, A.R. Rezvani, New silver(I) complex with diazafluorene based ligand: synthesis, characterization, investigation of *in vitro* DNA binding and antimicrobial studies, J. Mol. Struct. 1139 (2017) 407–417.

[50] M.T. Bilkan, Ş. Yurdakul, Z. Demircioğlu, O. Büyükgüngör, Crystal structure, FT-IR, FT-Raman and DFT studies on a novel compound $[C_{10}H_9N_3]_4AgNO_3$, J. Organomet. Chem. 805 (2016) 108–116.

[51] O. Noureddine, N. Issaoui, M. Medimagh, O. Al-Dossary, H. Marouani, Quantum chemical studies on molecular structure, AIM, ELF, RDG and antiviral activities of hybrid hydroxychloroquine in the treatment of COVID-19: molecular docking and DFT calculations, J. King Saud Univ. Sci. 33 (2021) 101334.

[52] I. Rozas, I. Alkorta, J. Elguero, Behavior of ylides containing N, O, and C atoms as hydrogen bond acceptors, J. Am. Chem. Soc. 122 (45) (2000) 11154–11161.

[53] H.A. El-Mageed, F.M. Mustafa, M.K. Abdel-Latif, Boron nitride nanoclusters, nanoparticles and nanotubes as a drug carrier for isoniazid anti-tuberculosis drug, computational chemistry approaches, J. Biomol. Struct. Dyn. (2020) 1–10.

[54] E.R. Johnson, S. Keinan, P. Mori-Sanchez, J. Contreras-García, A.J. Cohen, W. Yang, Revealing noncovalent interactions, J. Am. Chem. Soc. 132 (2010) 6498–6506.

[55] B. Fathima Rizwana, J.C. Prasana, S. Muthu, C.S. Abraham, Molecular docking studies, charge transfer excitation and wave function analyses (ESP, ELF, LOL) on valacyclovir : a potential antiviral drug, Comput. Biol. Chem. 78 (2019) 9–17.

[56] V. Pophristic, L. Goodman, N. Guchhait, Role of lone-pairs in internal rotation barriers, J. Phys. Chem. 101 (1997) 4290–4297.

[57] F. Weinhold, Chemistry: a new twist on molecular shape, Nature 411 (2001) 539–541.

[58] G. Socrates, Infrared and Raman Characteristic Group Frequencies, 3rd ed., Wiley, New York, 2001.

[59] S. Janani, H. Rajagopal, S. Muthuc, S. Aayisha, M. Raja, Molecular structure, spectroscopic (FT-IR, FT-Raman, NMR), HOMO-LUMO, chemical reactivity, AIM, ELF, LOL and molecular docking studies on 1-Benzyl-4-(N-Boc-amino)piperidine, J. Mol. Struct. 1230 (2021) 129657.

[60] A.E. Reed, L.A. Curtiss, F. Weinhold, Intermolecular interactions from a natural bond orbital, donor-acceptor viewpoint, Chem. Rev. 88 (1988) 899–926.

[61] J.P. Foster, F. Weinhold, Natural hybrid orbitals, J. Am. Chem. Soc. 102 (1980) 7211–7218.

[62] T. Aycan, F. Öztürk, T. Doruk, S. Demir, M. Fidan, H. Paşaoğlu, Synthesis, structural, spectral and antimicrobial activity studies of copper-nalidixic acid complex with 1,10-phenanthroline: DFT and molecular docking, Spectrochim. Acta Part A 241 (2020) 118639.

[63] F. Rizwana, J.C. Prasanaa, S. Muthu, C.S. Abraham, Molecular docking studies, charge transfer excitation and wave function analyses (ESP, ELF, LOL) on valacyclovir : a potential antiviral drug, Comput. Biol. Chem. 78 (2019) 9–17.

[64] S. Muthu, T. Rajamani, M. Karabacak, A.M. Asiri, Vibrational and UV spectra, first order hyperpolarizability, NBO and HOMO–LUMO analysis of 4-chloro-N-(2-methyl-2,3-dihydroindol-1-yl)-3-sulfamoyl-benzamide, Spectrochim. Acta Part A 122 (2014) 1–14.

[65] T. Hannah Clara, S. Muthu, J. C.Prasana, Quantum mechanical, spectroscopic and docking studies of (2E)-1-(4-aminophenyl)-3-(4-benzyloxyphenyl)-prop-2-en-1-one Chalcone derivative by density functional theory – A prospective respiratory drug, Mater. Today Proc. (2020).

[66] E. Thomas, K.P. Vijayalakshmi, B.K. Geaorge, Kinetic stability of imidazolium cations and ionic liquids: a frontier molecular orbit approach, J. Mol. Liquids 276 (2019) 720–727.

[67] N. Swarnalatha, S. Gunasekaran, S. Muthu, M. Nagarajan, Molecular structure analysis and spectroscopic characterization of 9-methoxy-2H-furo[3,2-*g*]chromen-2-one with experimental (FT-IR and FT-Raman) techniques and quantum chemical calculations, Spectrochim. Acta Part A 137 (2015) 721–729.
[68] A. Viji, B. Revathi, V. Balachandran, S. Babiyana, B. Narayana, V.V. Salian, Analysis of spectroscopic, quantum chemical calculations, molecular docking, RDG, ELF, anticancer and antimicrobial activity studies on bioactive molecule 2-[3-(4-*Chlorophenyl*)-5-(4-(*propane*-2-*yl*) *phenyl*-4,5- *dihydro*-1H-*pyrazol*-1-*yl*]-4-(4-methoxyphenyl)-1,3-thiazol, Chem. Data Collect. 30 (2020) 100585.
[69] F.K. Ommenya, E.A. Nyawade, D.M. Andala, J. Kinyua, Synthesis, characterization and antibacterial activity of schiff base, 4-chloro-2-{(E)-[(4-F*luorophenyl*)*imino*]methyl}phenol metal (II) complexes, J Chem. 8 (2020).
[70] M.L. Beatrice, S.M. Delphine, M. Amalanathan, M.S.M. Mary, H.M. Robert, K.T. Molf, Molecular structure, spectroscopic, Fukui function, RDG, anti-microbial and molecular docking analysis of higher concentration star anise content compound methyl 4-methoxybenzoate-DFT study, J. Mol. Struct. 1238 (2021) 130381.
[71] P.K. Chattaraj, B. Maiti, U. Sarkar, Philicity: a unified treatment of chemical reactivity and selectivity, J. Phys. Chem. A 107 (2003) 4973–4975.
[72] C. Morell, A. Grand, A. Toro-Labbe, New dual descriptor for chemical reactivity, J. Phys. Chem. A 109 (2005) 205–212.
[73] J.A. Mendoza, R.Y. Pineda, M. Nguyen, M. Tellez, A.M. Awad, Molecular docking studies, insilico ADMET predictions and synthesis of novel PEGAnucleosides as antimicrobial agents targeting class B1 metalloβlactamases, In Silico Pharmacol. 9 (2021) 33.
[74] A. Victoria, N. Elangovan, T. Gobi, S. Sowrirajan, T. Kolochi, Antitubercular activity of some new azomethine compounds, Int. J. Adv. Res. Biol. Sci. 4 (1) (2017) 44–52.
[75] X. Zhao, T.D Z.Yu, Quorum-sensing regulation of antimicrobial resistance in bacteria, Microorganisms. 8 (3) (2020) 425.
[76] W. Chu, D.A. Vattem, V. Maitin, M.B. Barnes, R.J. McLean, Bioassays of quorum sensing compounds using *Agrobacterium tumefaciens* and *chromobacterium violaceum*, Methods Mol. Biol. 692 (2011) 3–19.